ARCHIVE OF MECHANICAL ENGINEERING

DOI: 10.24425/ame.2024.151332 Early Access; pp. 445–466

Dung Van NGUYEN [1], Viet Quy BUI [1]

The effect of muzzle devices on the distribution of muzzle waves when firing an assault rifle

Received 23 February 2024, **Revised** 19 August 2024, **Accepted** 30 August 2024, **Published online** 26 September 2024

Keywords: muzzle wave, muzzle flow, muzzle device, acoustic impact, final effect period, assault rifle

When firing an infantry gun, the muzzle wave will spread into the surrounding space, which will cause harmful mechanical effects to the shooter and military personnel near the weapon. The impact of the muzzle wave on the shooter is increased when a muzzle device is placed on the barrel of the gun. Therefore, weapon designers desire to improve the efficiency of muzzle devices and limit the mechanical impact of the muzzle wave on the shooter's hearing organs. This article discusses a thermo-gasdynamic method for determining the changes in excess pressure distribution of the muzzle wave and sound pressure level at the shooter's ear position. The calculations focus on shooting an assault rifle with three different types of muzzle devices, each with varying features and efficiencies, using 7.62×39 mm ammunition. The results indicate that the isobaric curve of the muzzle wave shifts backward when a muzzle device is used. This shift can lead to an increase of up to 6 dB in the sound pressure level near the gunner's ear. The results of the mathematical models are consistent with the data from the experiments. The article provides a basis for a comprehensive quantitative assessment of the effectiveness of using muzzle devices.

1. Introduction

A muzzle device plays a very important role in controlling the stability of small and medium-sized hand-held weapons. These devices are parts or devices arranged at the muzzle of the barrel, working in the final effect period of gunpowder gas and utilizing the energy of this gas leaving out of the muzzle following the bullet to serve for various operational purposes of barreled weapons. Therefore, many studies on muzzle devices have been conducted [1–10]. Studies mainly focus on

✉ Viet Quy BUI, e-mail: buiquyviet@lqdtu.edu.vn

[1] Faculty of Special Equipment, Le Quy Don Technical University, Hanoi, Vietnam

evaluating the effectiveness of muzzle devices and the thermodynamic processes inside the device [1–5]. In the other direction, numerical methods were performed on guns with a muzzle device to analyze the influence of the structure and mass of the muzzle device on the behavior of the gun barrel at the moment the bullet leaves the barrel [6–9]. In addition, there was a research on the appropriate combination of parameters for a highly effective muzzle brake and shock absorber to reduce the recoil force of small-caliber automatic guns [10].

The outflow of gunpowder gas from the bore into the atmosphere occurs at high speeds, resulting in the formation of a shock wave at the muzzle of the barrel. If an automatic gun attached to a muzzle device is fired, the flow characteristics exiting the muzzle will change due to the device's construction, resulting in a series change in the muzzle wave. Several numerical simulations of the impulsive noise generated by the complex gas flows escaping from the muzzle and the basic structures generating the impulsive noise were calculated. The interaction of shock waves emitted from the muzzle was illustrated in detail, and the mechanism of the muzzle flow field was analyzed [11–14]. These works provide references for studies on muzzle flash suppression, muzzle noise prediction, and optimization of muzzle brake designs [15, 16].

As the distance from the gunpowder gas region increases, the intensity of the muzzle wave and its propagation speed decrease, and the muzzle wave degenerates into a sound wave. This occurs mainly due to the increase in its surface. For automatic weapons, shots produce dangerously high sound levels [17, 18]. The peak sound pressure levels (SPL) at the shooter's ear typically range from 140 dB to 170 dB [18–20]. Therefore, acoustic characteristics and estimates of auditory risk due to gunshots next to the shooter have been evaluated in several studies [21, 22]. The maximum sound pressure level near the shooter's ear depends on several factors, one of which is the position of the muzzle or the proximity of the gunpowder gas exhaust to the ear. There were numerous reports of acoustic traumas in the form of immediate hearing loss with tinnitus when firing modified firearms including muzzle brakes and gas ports [22, 23]. Based on the results of measuring the impulse noise that occurs when firing from several gun models used in the Armed Forces of the Russian Federation and linking and comparing it with the maximum permissible sound level, it has been shown that during training and combat firing, the acoustic impacts of shots really threaten the health of military personnel [24].

In terms of experimental research, one of the works provided an insight into recent developments in the measurement, prediction and assessment of impulsive noise exposure and the mechanisms of hearing damage [25]. A series of measurements were used to compare the simulation results with the experimental ones. A study evaluated the effects of sound suppression, ammunition, and barrel length on AR-15 rifles. The results indicated that the use of muzzle brake devices can significantly increase exposure for the shooter, and the direct acoustic impact of the AR-15 must be considered during acoustic measurements to fully evaluate its overall efficacy [26]. Accurate determination of sound exposure under firing con-

ditions requires appropriate measurement equipment [27]. In the field of weapons, the activities of test subjects often change very quickly, so the measurement system is required to have a very high sampling frequency to be able to record results accurately [28].

The dynamic process of gunpowder gas moving at high speed in the muzzle gas region is characterized by the variation of the gunpowder gas mass and its non-equilibrium state. An accurate description of the actual movement process of the powder gas requires a close combination of thermodynamic relations with the equations of gas mechanics. Therefore, the thermogasdynamic theory used to describe the powder gas dynamic processes ensures the continuity and mutual connection between the movement processes of gunpowder gas and the change of its thermodynamic parameters. In addition, when using muzzle devices, weapon designers aim to improve their efficacy and limit the possible harmful effects of muzzle waves. As a result, this article will investigate this aspect based on determining the change in the isobaric curves of the gunpowder gas during the final effect period and calculating the sound pressure of the shot at the gunner's position when firing a rifle with different muzzle devices. The obtained theoretical and experimental results provide a basis for improving the structure to enhance the performance of the muzzle device, as well as deciding whether to use it in service.

2. Thermo-gas-dynamic model of gunpowder gas flow at the muzzle zone

2.1. Basic assumptions

As a foundation for building a mathematical model describing the final effect period of gunpowder gas from an automatic firearm, the following assumptions are used [29, 30]:

a) The final effect period is determined by the dynamic parameters at the moment when the bullet bottom leaves the muzzle of the gun barrel;
b) The gas flow is considered to be compressible, non-absorbable, continuous, and homogeneous;
c) The process of gunpowder gas flow is quasi-static, in which the muzzle gas state is characterized by the instantaneous values of the parameters;
d) Outflow velocity is in critical mode; no heat exchange occurs between the gunpowder gas and the compressed air layer on the contact surface;
e) The gunpowder gas region formed in front of the muzzle cross-section follows the point explosion theory with a variable radius of R;
f) The density of the gunpowder gas inside the muzzle region is the same at all points and only changes as a function of time ($\text{grad}\rho = 0$);
g) The instantaneous distribution of the gas flow velocity during the final effect period is linear;
h) The time the bullet travels in the muzzle device is relatively short and can be ignored.

2.2. Physical model

Consider a physical model of gas flow from a barrel cavity (Fig. 1). When the bullet moves to the muzzle device, the gunpowder gas begins to escape into the atmosphere through the rapidly expanding annular gap between the bullet and the exit port. On the other hand, the gunpowder gas also flows through the side windows of the muzzle device. For automatic firearms, the speed of the released gas at the moment the bullet leaves the barrel muzzle is generally smaller than the local speed of sound [29]. In this case, the velocity of the gas flow will continuously fluctuate and increase until a critical (stable) flow regime is established at the muzzle. The period of the oscillation phase is extremely short and can be ignored, and the steady phase is established as soon as the bullet travels about its caliber. The duration of the stabilization phase lasts until the value of the pressure in the bore is equal to the critical pressure (p_{cr} = 0.18 MPa).

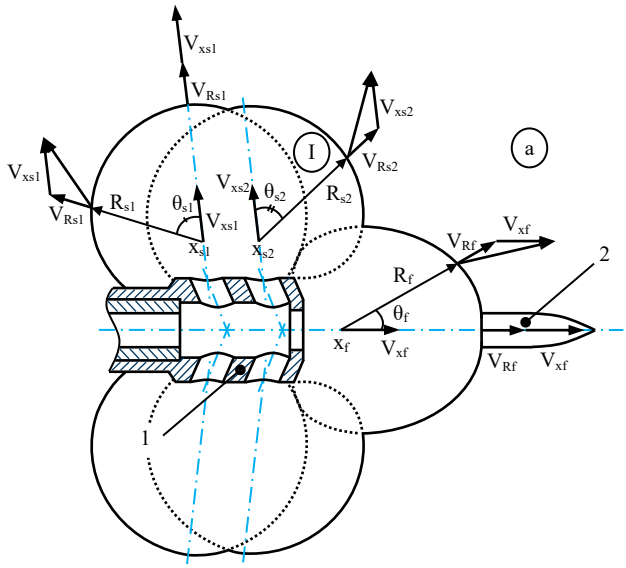

Fig. 1. Diagram for calculating the gunpowder gas region formed in front of the muzzle: 1 muzzle device; 2 bullet; a. atmosphere; I. expansion zone of gunpowder gas

The region of gunpowder gas flowing from the bore will move forward at the speed of the center of mass and will expand radially relative to the center of mass under the influence of momentum and excess pressure increased in it. The absolute speed of movement of points on the contact surface is different because their movement in relation to the muzzle cross-section is determined by the sum of two movements: translational movement with the speed of the center of mass and relative motion with the radial expansion speed of the gas region. Therefore, the energy of the gas zone will be transmitted to the muzzle wave with unbalanced

density in different directions determined by the polar angle θ_i from the gasflow axis (see Fig. 1). The index i indicates the direction of gas exit through the front hole, the first and the second side windows of the muzzle device (i indicates f, $s1$, $s2$). With the distance from the gas zone, the muzzle wave intensity will decrease, its propagation speed will decrease, and the muzzle wave will degenerate into sound.

When building the mathematical model, the Cartesian coordinate system Oxyz is arranged as follows:

Ox – the barrel axis is calculated from the cross section of the muzzle;

Oxz – firing plane;

Oxy – horizontal plane perpendicular to the Oxz plane.

Local coordinate systems $O_i x_i y_i z_i$:

$O_i x_i$ – gasflow axis from the side windows;

$O_i x_i z_i$ – vertical plane;

$O_i x_i y_i$ – horizontal plane.

2.3. Descriptive equations

The muzzle device attached to the automatic gun does not alter the mathematical model used to calculate the muzzle wave. However, the use of the muzzle device results in the gunpowder gas escaping not only forward but also through the holes and side windows. As a result, the parameters of the gas at the muzzle cross-section are replaced by the parameters of the gas at the cross-section of the gas outlet ports of the muzzle device.

To accurately determine these parameters of the gunpowder gas, it is necessary to calculate mutually interacting dynamic processes of the gas in the bore and the chambers of the muzzle device during the final effect period. Therefore, before creating a mathematical model for the thermogasdynamic process occurring in the space around the muzzle and creating muzzle waves, a mathematical model for calculating the state parameters of the gas in the chambers of the muzzle device must be determined [5]. This allows us to determine the different amounts of gas escaping in different directions of the muzzle device:

$$\frac{\mathrm{d}m_i}{\mathrm{d}t} = \mu_i F_i B(k) \frac{p_1}{\sqrt{RT_1}} \sqrt{1 - \left(\frac{p_a}{p_1}\right)^2} \tag{1}$$

with $B(k) = \left(\frac{2}{k+1}\right)^{\frac{k+1}{2(k-1)}} \sqrt{k}$;

where m_i – mass of gas exiting through the forward hole, the first and the second side windows of the muzzle device; μ_i – the flow coefficient; F_i – the cross-sectional area of the front exit port and the side windows, respectively; p_1, T_1– the gas pressure and temperature of the powder gas in the muzzle device chamber; p_a – the barometric pressure; k – the heat capacity ratio of the powder gas, and R –

the gas constant. The calculation for the state parameters of the gas in the chamber of the muzzle device is shown in Appendix.

The problem of calculating the characteristics of the muzzle wave around the muzzle is solved through sequential calculations. First, a mathematical model of the thermogasdynamic processes occurring in the near-muzzle space during the expansion of the gas region and the formation of the muzzle wave is built. It serves to determine the main characteristic, the angular density of the muzzle wave energy. Which is the amount of energy expended by the gunpowder gas on the formation of the muzzle wave within a unit solid angle in the direction of its propagation, determined by the polar angle θ_i ($0 \leqslant \theta_i \leqslant 2\pi$). The approach to determine the maximum value of the angular density of the muzzle wave energy propagating in the direction specified by the polar angle θ_i is shown in Appendix and calculated by the following equation:

$$E(\theta_i)_m = \max \left[E_{R_i} + E_{X_i} \cos \theta_i \right]. \tag{2}$$

The changes over time of the contact surface radius and the coordinates of the mass center of the gas region relative to the barrel muzzle cross-section are described:

$$\frac{\mathrm{d}R_i}{\mathrm{d}t} = V_{R_i}, \quad \frac{\mathrm{d}X_i}{\mathrm{d}t} = V_{X_i}. \tag{3}$$

Next, based on the calculated dependence of the angular density of the muzzle wave $E(\theta_i)$ and the coordinates of the mass center of the gas region on the polar angle θ_i, the spatial distribution field of the excess pressure Δp_{fs}, the excess pressure pulse i_+, and the duration of the compression stage Δt_+ is calculated (see Fig. 2). In general, these are the basic parameters characterizing the dynamic impact of the muzzle wave on the objects located near the muzzle.

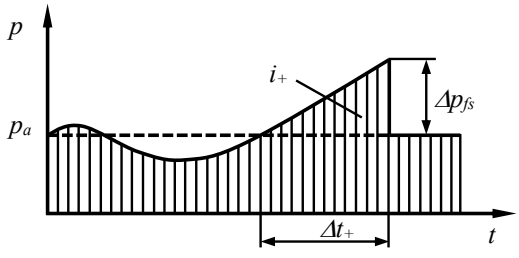

Fig. 2. Diagram of muzzle wave parameters

*** Calculating isobaric curves of the muzzle wave:**

With known values of the angular density of the muzzle wave energy $E(\theta_i)_m$ and the coordinates of the centers of its formation X_i depending on the polar angle (equations (2), (3)), we will calculate the coordinates of the location of the isobaric curves in the planes passing through the Ox axis with given values of

excess pressure at the wavefront. The radius of the muzzle wave with a given value of excess pressure can be determined using the linear polar coordinate:

$$r_{2i}(\theta_i) = f\,[E(\theta_i)_m] \qquad \text{when} \quad \Delta p_{fs} = \text{const.} \tag{4}$$

Relative pressure on the wave front surface according to the value of the given excess pressure Δp_{fs}:

$$\frac{p_2}{p_a} = 1 + \frac{\Delta p_{fs}}{p_a}\,. \tag{5}$$

The corresponding dimensionless radius of the muzzle wave R_2 is from the value of the relative pressure p_2/p_a [30]:

$$R_2 = f\left(\frac{p_2}{p_a}\right). \tag{6}$$

The radius of the muzzle wave $r_2(\theta_i)$ for the polar angle θ_i, where there is relative pressure p_2:

$$r_2(\theta_i) = \sqrt[3]{\frac{4\pi E(\theta_i)_m}{p_a}}R_2\,. \tag{7}$$

We can use the last formula to calculate the radius of the muzzle wave for all angles in the range of $\theta < \theta_i < \pi$; and according to the obtained linear polar coordinates of the mass center $X_i(\theta_i)$ on the $\mathrm{O}_i\mathrm{x}_i$ axis, we can find the coordinates of the points on the isobaric curve. This process can be repeated for different levels of excess pressure at the muzzle wavefront.

*** Calculating parameters of the muzzle wave at the position of the gunner's ear:**

The main parameter of the muzzle wave, determining its dangerous impact on human hearing organs, is the maximum value of excess pressure at the wave front. The peak sound pressure level L_m is measured in decibels:

$$L_m = 20\log\frac{\Delta p_{fs}}{p_0}\,, \tag{8}$$

where $p_0 = 2 \cdot 10^{-5}$ Pa – the receiving pressure at the audible level at 1000 Hz.

The excess pressure at the reference point (the gunner's ear) need to be determined. In the case of a gun fitted with a muzzle device, calculations are made for the side window of the device closest to the shooter and the side window with the highest energy release.

The excess pressure at the wave front follows the relationship from Eq. (5):

$$\Delta p_{fs} = \left(\frac{p_2}{p_a} - 1\right)p_a\,. \tag{9}$$

In the theory of point explosion [30], it was established that the parameters of the shock wave are described with sufficient accuracy by the following asymptotic dependencies:

$$\frac{p_2}{p_a} = 1 + \frac{0.227}{R_2\sqrt{\lg R_2 + 0.158}}, \tag{10}$$

$$J_+ = \frac{0.038}{R_2}, \tag{11}$$

$$\Delta\tau_+ = 0.192\sqrt{R_2}. \tag{12}$$

The dimensionless radius of the muzzle wave corresponds to the relation:

$$R_{2i} = \sqrt[3]{\frac{p_a}{4\pi E(\theta_i)_m}}\, r_{2i}. \tag{13}$$

The polar angle of the reference point:

$$\theta_{ri} = \arccos \frac{x_{ri} - x(\theta_i)_m}{\sqrt{x_{ri}^2 + y_{ri}^2 + z_{ri}^2}}, \tag{14}$$

where $(x_{ri},\ y_{ri},\ x_{ri})$ – the reference point coordinates in coordinate systems $O_i x_i y_i z_i$.

The radius of the muzzle wave by the time it gets to the reference point:

$$r_{2i} = \sqrt{[x_{ri} - x(\theta_i)_m]^2 + [y_{ri} - y(\theta_i)_m]^2 + [z_{ri} - z(\theta_i)_m]^2}. \tag{15}$$

Equations (8)–(15) help us determine the sound pressure level at the shooter's ear position.

Other parameters of the muzzle wave at the gunner's ear position are determined [29]:

$$i_+ = p_a\sqrt{\frac{\rho_a}{p_a}}\sqrt[3]{\frac{E_{0i}}{p_a}}J_+, \tag{16}$$

$$\Delta t_+ = \sqrt{\frac{\rho_a}{p_a}}\sqrt[3]{\frac{E_{0i}}{p_a}}\Delta\tau_+ \tag{17}$$

with the total energy of the gunpowder gas spent on the formation of the muzzle wave that is determined by the whole solid angle of the gas radial expansion, equal to 4π:

$$E_{0i} = \sum 4\pi E_{R_i} \quad (\text{when } \theta_i = \pi/2), \tag{18}$$

The permissibility of acoustic impact when shooting from small arms without means of hearing protection is determined on the basis of an equal loudness curve, the approximation of which has the form [29]:

$$[L] = 185 - 9.5 \times \log \frac{0.0125}{\Delta t_+}. \tag{19}$$

Usable muzzle devices without protection must satisfy:

$$L_m \leqslant [L]. \tag{20}$$

3. The influence of muzzle devices on muzzle waves when shooting an assault rifle

3.1. Initial data

To illustrate the presented calculation method, we will calculate the muzzle wave characteristics and sound pressure at the position of the gunner's ear when shooting from a 7.62 mm caliber automatic gun with and without muzzle devices. At the points mentioned above, the sound pressure level of the muzzle wave will be measured using instruments. In terms of initial data, we will use the gas parameters at the muzzle cross-section, calculated according to the results of the internal ballistics problem, whose calculation results are shown in Fig. 3 and Table 1.

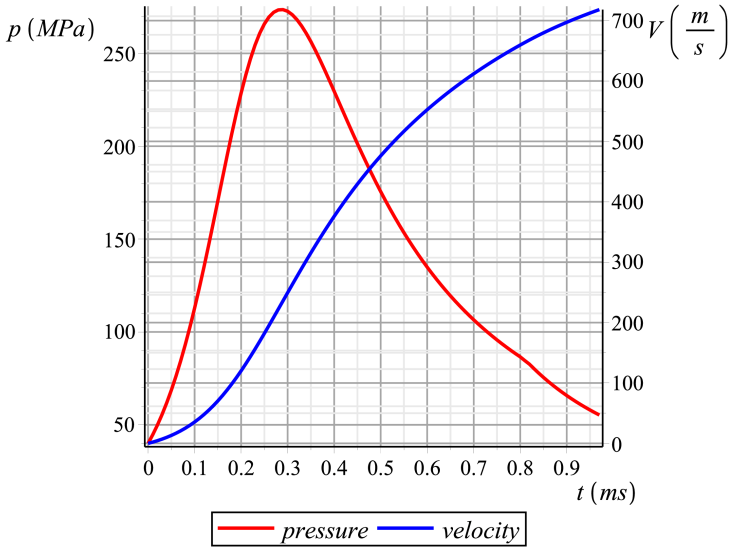

Fig. 3. Graph of gunpowder gas pressure and bullet velocity in the bore

The initial conditions of the differential equations in the system are the correlations when $t = t_d$ according to Table 2.

Table 1. Gas parameters at the muzzle cross-section

Parameter	V_d (m/s)	p_d (N/m^2)	ρ_d (kg/m^3)	a_d (m/s)	t_d (s)
Value	719	$52 \cdot 10^6$	70.78	942	$0.97 \cdot 10^{-3}$

Table 2. Genaral data

Parameter	Value	Parameter	Value	Parameter	Value	Parameter	Value
d (m)	$7.62 \cdot 10^{-3}$	k_a	1.4	$\Im_0$ (J)	$9.4 \cdot 10^{-2}$	X_{i0} (m)	0
l_d (m)	0.37	p_a (N/m^2)	$101.3 \cdot 10^3$	$R_{\phi 0}$ (m)	$\sqrt{S_\phi/\pi}$	E_{Ri} (J)	0
S (m^2)	$47.6 \cdot 10^{-6}$	ρ_a (kg/m^3)	1.225	V_{R0} (m/s)	0	E_{Xi} (J)	0
k	1.25	m_0 (kg)	$0.28 \cdot 10^{-6}$	J_{Xi0} (Ns)	0		

Other data for calculating muzzle waves for the assault rifle with different muzzle devices are according to Table 3.

Table 3. Structural parameters of muzzle devices

Parameter	Multi-window muzzle brake	2-wall muzzle brake compensator	Adjustable muzzle brake compensator
S_ϕ (m^2)	$50.26 \cdot 10^{-6}$	$63.62 \cdot 10^{-6}$	$63.62 \cdot 10^{-6}$
S_{w1} (m^2)	$12.57 \cdot 10^{-6}$	$251.33 \cdot 10^{-6}$	$9.62 \cdot 10^{-6}$
n_1	20	1	5
S_{w2} (m^2)	0	$251.33 \cdot 10^{-6}$	$170.27 \cdot 10^{-6}$
n_2	0	1	3
ψ_{en} (°)	90	90	90
ψ_{ex} (°)	90	131	90
ψ_c (°)	90	41; 33	20; 23

3.2. Results

Numerical methods were used to solve differential equations. The Maple program accurately calculated the isobaric lines for both firing a 7.62 mm automatic gun with and without muzzle devices, as depicted in Figs. 4 to 7 (the coordinate axis unit is meter).

As can be seen from the graphs, the muzzle wave propagating in the air has a shape similar to a unidirectional cardioid. In the case of a muzzle device, a clear directionality of the muzzle wave can be observed from the center point of the muzzle section. In the case of no muzzle device, the results are different. It is shown that the muzzle device changes the structure of the flow field, thereby affecting pressure field propagation. The muzzle device shifts the muzzle wave field backwards. With muzzle devices designed to create compensating forces on the plane of firing, there is an asymmetry in the isobaric lines. As the excess pressure on the muzzle wavefront gradually decreases, the isobaric curve gradually approaches a circular shape, according to the point explosion theory.

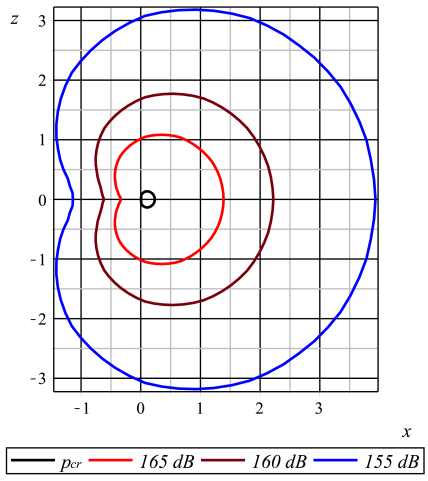

Fig. 4. Isobaric field distribution on the muzzle wave front in the case without a muzzle device

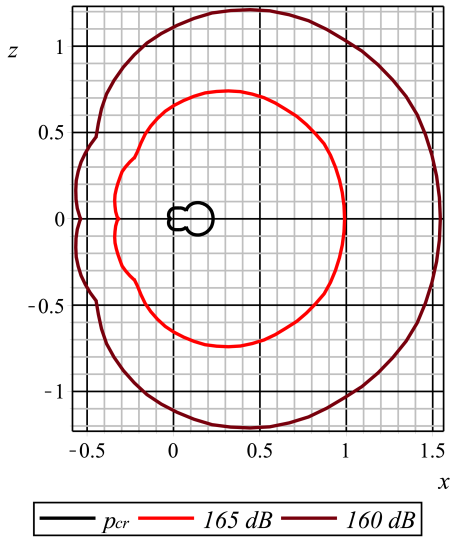

Fig. 5. Isobaric field distribution on the muzzle wave front when using a multi-window muzzle brake

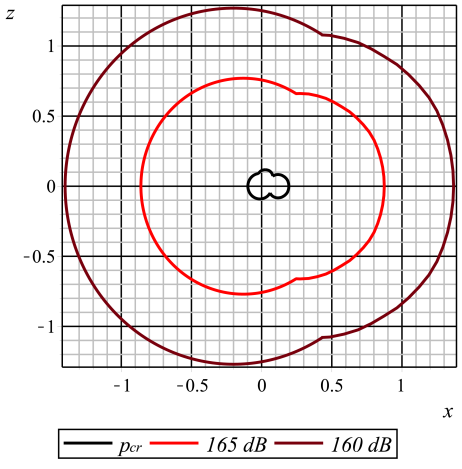

(a) on the firing plane

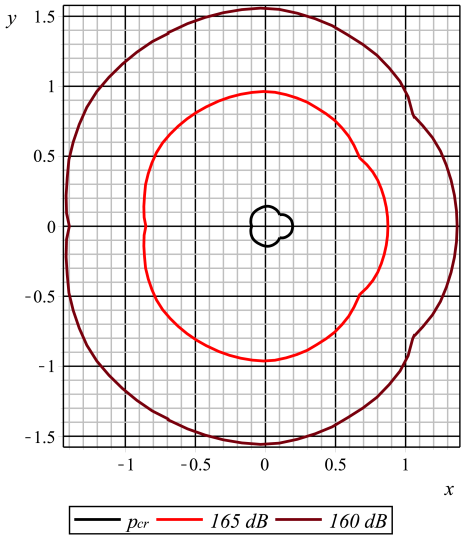

(b) on the horizontal plane

Fig. 6. Isobaric field distribution on the muzzle wave front when using a 2-wall muzzle brake compensator

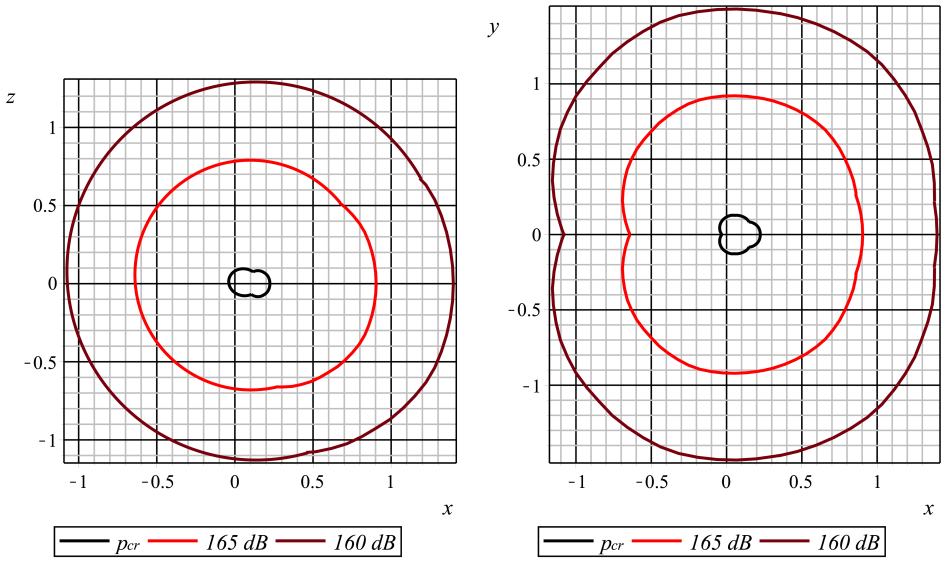

(a) on the firing plane

(b) on the horizontal plane

Fig. 7. Isobaric field distribution on the muzzle wave front when using an adjustable muzzle brake compensator

The calculated values of excess pressure at locations with a radius of 1.0 m and angles of 60°, 90°, and 135° counterclockwise compared to the firing direction are shown in Table 4. Control parameters to evaluate the possibility of using a muzzle device are shown in bold in the below part of the table. It can be seen that the

Table 4. Results of the excess pressure calculation around the muzzle

Parameter	Gun without the muzzle device	Multi-window muzzle brake	2-wall muzzle brake compensator	Adjustable muzzle brake compensator
Point r = 1 m, θ = 60°				
Δp (Pa)	5196	2843	2958	3039
Point r = 1 m, θ = 90°				
Δp (Pa)	4245	2457	3170	3125
Point r = 1 m, θ = 135°				
Δp (Pa)	2880	1704	3216	2918
Point r = 0.83 m, θ = 172°				
i_+ (Pa s)	0.066	0.068	0.199	0.127
Δt_+ (s)	$0.157 \cdot 10^{-3}$	$0.158 \cdot 10^{-3}$	$0.206 \cdot 10^{-3}$	$0.185 \cdot 10^{-3}$
***Lm* (dB)**	**159**	**159**	**165**	**163**
***[L]* (dB)**	**167**	**167**	**168**	**168**

sound pressure levels reaching the gunner's ears are in the range of 159–165 dB. However, the time of the compression phase is relatively small compared to the time of the final effect period, about $4 \cdot 10^{-3}$ s.

4. Experiment

4.1. Experimental setup

The test was conducted by the Weapons Experimental Center at Le Quy Don Technical University in Vietnam. The experimental equipment structure includes a 7.62 mm caliber assault rifle, placed on a specialized rack with a reverse block and linkage to limit errors due to the shooter's actions while ensuring the most realistic description of typical shooting conditions.

The testing system mainly includes an acoustic sensor, excess pressure sensors, signal analysis, and a display system. Fig. 8 shows a photograph of the experimental setup. The excess pressure sensors were mounted on tripods that were adjusted to ensure the level with the barrel axis throughout the test, approximately 1.2 m above the ground. The sound sensor is placed on a shelf corresponding to the control position presented above.

Fig. 8. Experimental equipment arrangement

Excess pressures were measured at locations with a radius of 1.0 m and angles of 60°, 90°, and 135° counterclockwise from the firing direction. An overview of the measurement points and the corresponding field diagram is shown in Fig. 9.

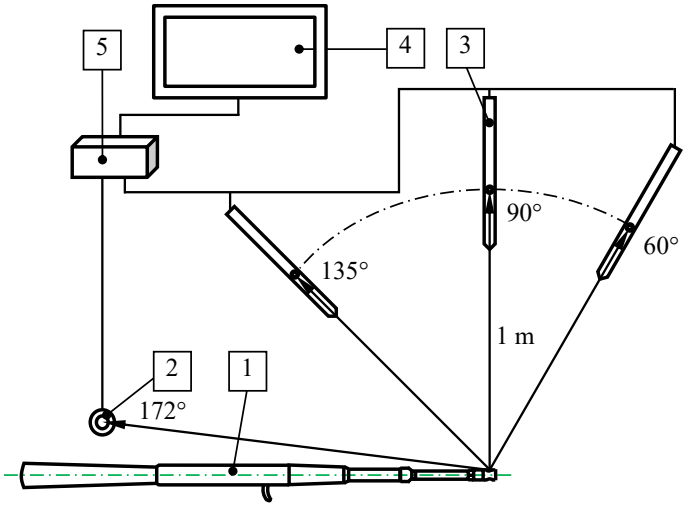

Fig. 9. Block diagram of the test system on the horizontal plane: 1 measuring object (gun); 2 sound sensor; 3 excess pressure sensor; 4 display device; 5 signal analyzer

The muzzle devices mounted on the assault rifle were used in the evaluation tests, as shown in Fig. 10.

(a) multi-window muzzle brake

(b) 2-wall muzzle brake compensator

(c) adjustable muzzle brake compensator

Fig. 10. Experimental muzzle devices

4.2. Experimental results

In the experiment, the same behavior was observed in all shots, so the results from the case where the gun was fitted with an adjustable muzzle device were taken as an example to clarify. The excess pressure varies with time at different measurement points, as shown in Fig. 11.

The averages of the excess pressure and the peak sound pressure level at all the measurement points are shown in Table 5.

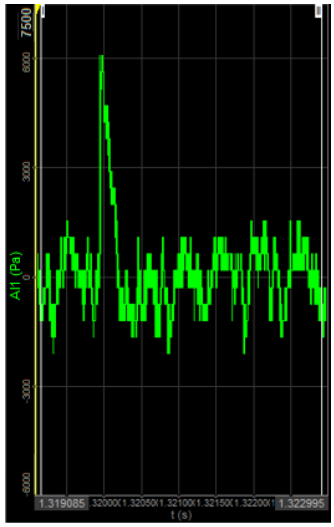

(a) At the point $\theta = 60^\circ$

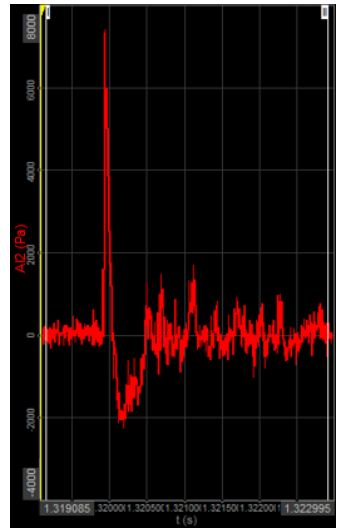

(b) At the point $\theta = 90^\circ$

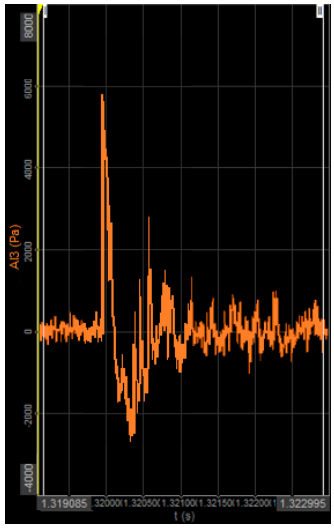

(c) At the point $\theta = 135^\circ$

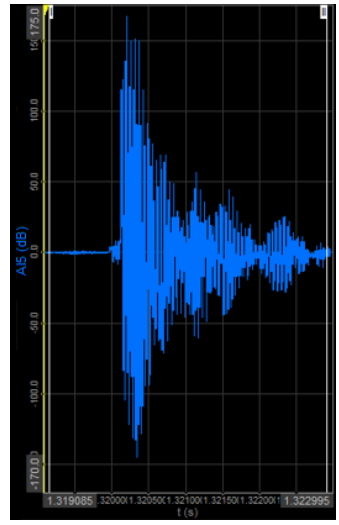

(d) At the point $\theta = 172^\circ$

Fig. 11. Graph of the excess pressure and the peak sound pressure

The value of this difference varies with the type of muzzle device and measurement position. As shown in Table 5, the difference in the peak sound pressure of the weapon tested in this study was between 159 and 166 dB (error 0 to 3.4%). For the 2-wall muzzle brake compensator, both the calculated and experimental values of the peak sound pressure at the gunner's ear position are all higher than the other options, since the structure of this device has a 163° angle to the air jet.

Table 5. Comparison of theoretical and experimental results for the excess pressure

Parameter Δp (Pa)	Gun without the muzzle device	Multi-window muzzle brake	2-wall muzzle brake compensator	Adjustable muzzle brake compensator
Point $\theta = 60^\circ$				
Experimental result	5026	2800	3029	3139
Theoretical result	5196	2843	2958	3039
Error (%)	3.4	1.5	2.3	3.2
Point $\theta = 90^\circ$				
Experimental result	4176	2452	3254	3123
Theoretical result	4245	2457	3170	3125
Error (%)	1.7	0.2	2.6	0.1
Point $\theta = 135^\circ$				
Experimental result	2946	1740	3322	2916
Theoretical result	2880	1704	3216	2918
Error (%)	2.2	2.1	3.2	0.1
Lm (dB) at the point $\theta = 172^\circ$				
Experimental result	160	159	166	163
Theoretical result	159	159	165	163
Error (%)	0.6	0	0.6	0

5. Conclusions

This article establishes a mathematical model that describes the expansion process of gunpowder gas and the formation of muzzle waves using the thermogas-dynamic theory. This model merges with the mathematical model describing the dynamic process of the gunpowder gas occurring in the barrel, in the gas chamber of the gas engine, and in the muzzle device. The merged model ensures the continuity and mutual relationship between the movement processes of the gunpowder gas.

The calculations focus on determining the changes in excess pressure distribution of the muzzle wave and the sound pressure level at the shooter's ear position when firing a small-caliber automatic gun with different types of muzzle devices. The calculated results include both the numerical values and visual representations of how the muzzle device affects the muzzle wave by shifting the isobaric curve backward. This results in an increase in the sound pressure level near the shooter's ear, making it crucial to consider this when designing or using muzzle devices, particularly those with reverse jet airflow.

The deviation between the calculated results and the experimental data is relatively small, indicating that the theoretical model is accurate and reliable. However, the calculated results only show the isobaric curves at certain points at a time, so further work requires calculating the muzzle wave variation over time and determining the optimal structure of the muzzle device.

The research is useful in more thoroughly assessing the influence of a muzzle brake on muzzle waves when used. As a result, this article provides a comprehensive perspective on the usage of the muzzle devices, as well as a useful reference for designing muzzle devices for small-caliber gun systems.

Appendix

*** Equations describing the thermogasdynamic process in the muzzle device:**

The mathematical model includes the following groups of equations [5]. The equations for changing the mass and internal energy of the gas in the muzzle device chamber:

$$\frac{\mathrm{d}m}{\mathrm{d}t} = \frac{\mathrm{d}m_d}{\mathrm{d}t} - \sum \frac{\mathrm{d}m_i}{\mathrm{d}t}, \tag{21}$$

$$\frac{\mathrm{d}U_1}{\mathrm{d}t} = H_0 \frac{\mathrm{d}m_d}{\mathrm{d}t} - H_1 \sum \frac{\mathrm{d}m_i}{\mathrm{d}t} - \frac{\mathrm{d}Q}{\mathrm{d}t}, \tag{22}$$

where m, m_d – mass of the gas in the muzzle device chamber, mass of gas from the barrel into the muzzle device; U_1 – internal energy of the gas in the muzzle device chamber; H_0, H_1 – gas energies for specific flows in the barrel, in the muzzle device.

Equation of gas energy for specific flows:

$$H_j = \frac{k}{k-1} R T_j \quad (j = 0.1). \tag{23}$$

Energy loss of the powder gas due to heat transfer:

$$\frac{\mathrm{d}Q}{\mathrm{d}t} = \alpha \frac{T_1 F - \dfrac{4}{3\sqrt{\pi} v_\tau} \dfrac{Q}{\sqrt{t}}}{1 + \alpha \dfrac{2}{3\sqrt{\pi} v_\tau} \sqrt{t}}, \tag{24}$$

where v_τ – the heat absorption coefficient; F – the heat transfer surface area; and α – the heat transfer coefficient.

The equations for the gas state parameters in the device chamber:

$$p_1 = (k-1) \frac{U_1}{W_1}, \tag{25}$$

$$T_1 = \frac{k-1}{R} \frac{U_1}{m}, \tag{26}$$

where W_1 – the volume of the device chamber.

The equations for the change in mass of the gas flow from the barrel into the muzzle device:

$$\frac{\mathrm{d}m_d}{\mathrm{d}t} = \begin{cases} \mu_d S B(k) \dfrac{p_d}{\sqrt{RT_d}} \sqrt{1 - \left(\dfrac{p_1}{p_d}\right)^2} & \text{when } p_d \geqslant p_1\,, \\ 0 & \text{when } p_d < p_1\,, \end{cases} \tag{27}$$

where S – the cross-sectional area of the bore; p_d, T_d – the pressure and temperature of the powder gas at the muzzle; μ_d – the flow coefficient of the gas flow from the bore to the muzzle device.

*** Equations describing the thermogasdynamic process in the gas expansion zone:**

To build a system of equations representing the mathematical model of thermogasdynamic processes when there is radial expansion and translational motion in the gas region, we will use the differential form of the equations of the conservation of mass, energy, and momentum.

When applied to the muzzle gas region, the equation for the total energy change of the gunpowder gas according to the conservation law of energy:

$$\frac{\mathrm{d}\Im_i}{\mathrm{d}t} = H_1 \frac{\mathrm{d}m_i}{\mathrm{d}t} - 4\pi R_i^2 p_{R_i} V_{R_i}\,. \tag{28}$$

In this formula, $\Im_i$ – total kinetic and internal energy of the gas in the gas regions; m_i – the gas mass in the gas regions; p_{Ri} – the pressure of the gunpowder gas on the surfaces; R_i – the radius of the gunpowder gas regions.

To obtain the equation for the change in velocity of the radial motion of the points on the contact surface, we consider the change in momentum of a compressed layer of air on the contact surface as the gas region expands:

$$\frac{\mathrm{d}}{\mathrm{d}t}\left(m_a V_{R_i}\right) = 4\pi R_i^2 \left(p_{R_i} - p_a\right), \tag{29}$$

where m_{ai} – the mass of air in the volume occupied by the gunpowder gas.

$$m_{ai} = \frac{2\,(k_a + 1)}{3} \pi \rho_a R_i^3\,. \tag{30}$$

Differentiating the expression of the momentum in the bracket on the left side, we obtain after transformations the equation for changing the radial velocity of points on the air contact surface [30]:

$$\frac{\mathrm{d}V_{R_i}}{\mathrm{d}t} = \frac{6}{k_a + 1} \frac{p_{R_i} - p_a}{\rho_a R_i} - \frac{3V_{R_i}^2}{R_i}\,, \tag{31}$$

where k_a – the heat capacity ratio of the air; ρ_a and p_a – air density and pressure.

The change in momentum of the gas region during its translational movement together with the spherical layer of compressed air on the contact surface in the direction of the momentum vector of the powder gas flowing out of the muzzle device:

$$\frac{\mathrm{d}J_{X_i}}{\mathrm{d}t} = \mu_i F_i \left\{ [p_1 - p_a] + \rho_1 V_1^2 \right\} \left(1 - \frac{F_i}{\pi R_i^2} \right) - \frac{\pi \rho_a}{2} R_i^2 V_{X_i}^2 \,. \tag{32}$$

The velocity of the mass center of gunpowder gas, V_{Xi} is calculated:

$$V_{X_i} = \frac{J_{X_i}}{m_i + m_{ai}} \,. \tag{33}$$

The average value of pressure in the gunpowder gas region under the assumption $\mathrm{grad}\rho = 0$ is determined:

$$\bar{p}_i = (k-1)\frac{3U_i}{4\pi R_i^3} \,, \tag{34}$$

where U_i – the internal energy of the gunpowder gas in the gas volume, is determined by subtracting the kinetic energy of the gas in relative and translational motion from its total energy:

$$U_i = \Im_i - E\left(m_i, V_{R_i}\right) - \frac{m_i}{2} V_{X_i}^2 \,, \tag{35}$$

where $E(m_i, V_{Ri})$ – the kinetic energy of the relative radial motion of the gunpowder gas in the gas region [29]:

$$E\left(m_i, V_{R_i}\right) = \int_0^{R_i} \rho_i \frac{v_r^2}{2} 4\pi r^2 \,\mathrm{d}r = \frac{3m_i}{2R_i^5} V_{R_i}^2 \int_0^{R_i} r^4 \,\mathrm{d}r = \frac{3}{10} m_i V_{R_i}^2 \,. \tag{36}$$

Differentiating with respect to time the equation (36), we find:

$$\frac{\mathrm{d}E\left(m_i, V_{R_i}\right)}{\mathrm{d}t} = \frac{3}{10} V_{R_i}^2 \frac{\mathrm{d}m_i}{\mathrm{d}t} + \frac{3}{5} m_i V_{R_i} \frac{\mathrm{d}V_{R_i}}{\mathrm{d}t} \,. \tag{a}$$

On the other hand, according to the integral form of the law of conservation of kinetic energy in the control volume at $\mathrm{grad}p = 0$, we have:

$$\frac{\mathrm{d}E\left(m_i, V_{R_i}\right)}{\mathrm{d}t} = 4\pi R_i^2 \left(\bar{p}_i - p_{R_i}\right) V_{R_i} \,. \tag{b}$$

By equating the right-hand sides of equations (a), (b), we obtain a differential expression for the radial velocity of the contact surface. Then, excluding the

derivative in the differential equation (31) using the expression obtained, after transforming which we obtain an equation that determines the pressure of the powder gas on the contact surface:

$$p_{R_i} = \frac{\frac{20}{3}\frac{\pi R_i^2}{m_i}\bar{p}_i + \frac{6}{k_a+1}\frac{1}{\rho_a R_i}p_a - \frac{1}{2}\frac{V_{R_i}}{m_i}\frac{\mathrm{d}m_i}{\mathrm{d}t} + \frac{3V_{R_i}^2}{R_i}}{\frac{20}{3}\frac{\pi R_i^2}{m_i} + \frac{6}{k_a+1}\frac{1}{\rho_a R_i}}. \tag{37}$$

After deriving the equation for the pressure on the contact surface, we compile equations that determine the increments of the angular density of the muzzle wave energy in the relative and translational motion of the contact surface:

$$\frac{\mathrm{d}E_{R_i}}{\mathrm{d}t} = R_i^2 V_{R_i} p_{R_i}, \quad \frac{\mathrm{d}E_{X_i}}{\mathrm{d}t} = R_i^2 V_{X_i} p_{R_i}. \tag{38}$$

The indicated increments are added up in the absolute motion of the contact surface points and form the angular density of the muzzle wave as a function of the polar angle θ_i ($0 \leqslant \theta_i \leqslant 2\pi$). The greatest intensity of the muzzle wave propagating in the direction of the polar angle θ_i is determined by the maximum value of the angular energy density in this direction.

Equations (2), (3), (28)–(38) form a general set of equations for the mathematical model for calculating the angular density of the muzzle wave energy.

References

[1] D.N. Zhukov, V.V. Chernov, and M.V. Zharkov. Development of an algorithm for calculating muzzle devices in the CFD package, fundamentals of ballistic design. In *All-Russian Scientific and Technical Conference*, pages. 126–129, St. Petersburg, Russia, 2012 (in Russian).

[2] R. Cayzac, E. Carettet, and T.A. De Roquefort. 3D unsteady intermediate ballistics modelling: Muzzle brake and sabot separation. In *Proceedings of the 24th International Symposium on Ballistics*, pages 423–430, New Orleans, LA, USA, 2008.

[3] J.S. Li, M. Qiu, Z.Q. Liao, D.P. Xian, and J. Song. Dynamic modeling and simulation of gatling gun with muzzle assistant-rotating and recoil absorber. *Acta Armamentarii*, 35(9):1344–1349, 2014. doi: 10.3969/j.issn.1000-1093.2014.09.003.

[4] H.H. Zhang, Zh.H. Chen, X.H. Jiang and H.Zh. Li. Investigations on the exterior flow field and the efficiency of the muzzle brake. *Journal of Mechanical Science and Technology*, 27:95–101, 2013. doi: 10.1007/s12206-012-1223-8.

[5] D.V. Nguyen, V.Q. Bui, D.T. Nguyen, Q.S. Uong, and H.T. Truong. Studying the thermo-gas-dynamic process in a muzzle brake compensator. *Archive of Mechanical Engineering*, 70(2):311–328, 2023. doi: 10.24425/ame.2023.145584.

[6] I. Semenov, P. Utkin, I. Akhmedyanov, I. Menshov, and P. Pasynkov. Numerical investigation of near-muzzle blast levels for perforated muzzle brake using high performance computing. In *International Conference "Parallel and Distributed Computing Systems" PDCS 2013*, pages 281–289, Kharkiv, Ukraine, March 13-14, 2013.

[7] M. Stiavnicky and P. Lisy. Influence of barrel vibration on the barrel muzzle position at the moment when bullet exits barrel. *Advances in Military Technology*, 8(1):89–102, 2013.

[8] N.Z. Ahmed, D.D. Jerković, N.P. Hristov, and W.B. Abaci. Analytical and experimental investigation of the muzzle brake efficiency. *Facta Universitatis, Mechanical Engineering*, 2023.

[9] H.L. Hua H, Zh.Q. Liao, and X.Y. Zhang. Muzzle dynamic characteristics analysis and its matching for firing accuracy improvement. *Journal of Vibration and Shock*, 36(8):29–33, 2017. (in Chinese).

[10] J.B. Xiao, G.L. Yang, H.Q. Li, M. Qiu, Zh.Q. Liao. Influence of matching muzzle brake and buffer on weapon recoil. *Journal of Ballistic*, 29(4):86–92, 2017.

[11] G. Klingenberg. Gun muzzle blast and flash. *Propellants, Explosives, Pyrotechnics*, 14(2):57–68, 1989. doi: 10.1002/prep.19890140204.

[12] Q. Luo and X. Zhang. Numerical simulation of serial launch process of multiple projectiles considering the aftereffect period. *International Journal of Numerical Methods for Heat & Fluid Flow*, 27(8):1720–1734, 2017. doi: 10.1108/hff-04-2016-0151.

[13] Y. Wang and X. Zhang. Numerical investigation on muzzle flow characteristics for small combustion chamber with embedded propelled body. *Structures*, 50:1783–1793, 2023. doi: 10.1016/j.istruc.2023.03.001.

[14] X.Y. Zhao, K.D. Zhou, L. He, Y. Lu, J. Wang, and Q. Zheng. Numerical simulation and experiment on impulse noise in a small caliber rifle with muzzle brake. *Shock and Vibration*, 2019:5938034, 2019. doi: 10.1155/2019/5938034.

[15] P.F. Li and X.B. Zhang. Numerical research on adverse effect of muzzle flow formed by muzzle brake considering secondary combustion. *Defence Technology*, 17(4):1178–1189, 2021. doi: 10.1016/j.dt.2020.06.019.

[16] J. Bin, M. Kim, and S. Lee. A numerical study on the generation of impulsive noise by complex flows discharging from a muzzle. *International Journal for Numerical Methods in Engineering*, 75(8):964–991, 2008. doi: 10.1002/nme.2291.

[17] C.G. Le Prell. Sound level suppressors for the reduction of firearm noise: implications for hearing conservation. *Canadian Audiologist*, 4(5), 2017.

[18] G.A. Flamme, M. Stewart, D. Meinke, J. Lankford, and P. Rasmussen. Auditory risk to unprotected bystanders exposed to firearm noise, *Journal of the American Academy of Audiology*, 22(2):93–103, 2011. doi: 10.3766/jaaa.22.2.4.

[19] J.E. Lankford, D.K. Meinke, G.A. Flamme, D.S. Finan, M. Stewart, S. Tasko, and W.J. Murphy. Auditory risk of air rifles. *International Journal of Audiology*, 55(sup1):S51–S58, 2016. doi: 10.3109/14992027.2015.1131851.

[20] V.K. Zelenko and A.I. Nesterenko. Analysis of advantages and disadvantages of modern muzzle devices for reducing the sound of a shot. *International Research Journal*, 12(102):63–70, 2020. doi: 10.23670/IRJ.2020.102.12.011 (in Russian).

[21] J.C. Freytag, D.R. Begault, and C.A. Peltier. The acoustics of gunfire. In *Inter-Naise 2006*, 10 pages, 2-6 Dec.2006, Honolulu, Hawaii, USA.

[22] D.K. Meinke, D S. Finan, G.A. Flamme, W.J. Murphy, M. Stewart, J.E. Lankford, and S. Tasko. Prevention of noise-induced hearing loss from recreational firearms. *Seminars in Hearing*, 38(04):267-281, 2017. doi: 10.1055/s-0037-1606323.

[23] R.M. Traynor, et al. Jump Start Your Practice with Recreational Audiology, *Hearing Health & Technology Matters*, 2020.

[24] M.A. Ryzhikov et al. Hygienic characteristics of impulse noise during firearms shooting, Experimental studies. *Bulletin of the Russian Military-Medical Academy*, 149-153, 2016 (in Russian).

[25] P. Teague, J. Conomos and V. Alexandrou. Overview of developments in the description and assessment of high intensity impulse noise exposure. In *Proceedings of ACOUSTICS 2016*, 10 pages, 9-11 Nov. 2016, Brisbane, Australia.

[26] E. Lobarinas, R. Scott, C. Spankovich,and C.G. Le Prell. Differential effects of suppressors on hazardous sound pressure levels generated by AR-15 rifles: Considerations for recreational shooters, law enforcement, and the military. *International Journal of Audiology*, 55(sup1):S59–S71, 2016. doi: 10.3109/14992027.2015.1122241.

[27] J. Selech, A. Kilikevičius, K. Kilikevičienė, S. Borodinas, J. Matijošius, D. Vainorius, J. Marcinkiewicz, and Z. Staszak. Force and Sound pressure sensors used for modeling the impact of the firearm with a suppressor. *Applied Sciences*, 10(3):961, 2020. doi: 10.3390/app10030961.

[28] P. VanDelden, P. Tsui,and A. Medemblik. Differences in Sound Exposure Results From Firearm Discharge Due to Measurement Equipment Selection, Canadian Acoustics [Internet], 2019 Oct. 16 [cited 2023 May 23], 47(3):86-7. Available from: https://jcaa.caa-aca.ca/index.php/jcaa/article/view/3351.

[29] Yu.P. Platonov. *Thermo-gas-dynamics of Automatic Weapons, Mechanical Engineering*, 2009 (in Russian).

[30] V.P. Korobeĭnikov. *Problems in the Theory of Point Explosion in Gases*. American Mathematical Society, 1976.